Journal of Colloid and Interface Science 641 (2023) 338–347

Contents lists available at ScienceDirect

Journal of Colloid and Interface Science

journal homepage: www.elsevier.com/locate/jcis

Amyloid fibril-nanocellulose interactions and self-assembly

Nico Kummer [a,b], Caroline E. Giacomin [b], Peter Fischer [b], Silvia Campioni [a,*], Gustav Nyström [a,b,*]

[a] Laboratory for Cellulose & Wood Materials, Empa – Swiss Federal Laboratories for Materials Science and Technology, Überlandstrasse 129, 8600 Dübendorf, Switzerland
[b] Institute of Food Nutrition and Health, Schmelzbergstrasse 9, ETH Zurich, 8092 Zurich, Switzerland

GRAPHICAL ABSTRACT

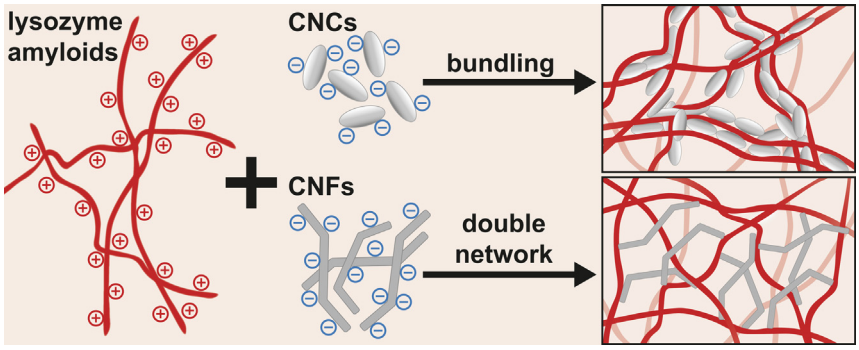

ARTICLE INFO

Article history:
Received 21 December 2022
Revised 20 February 2023
Accepted 1 March 2023
Available online 5 March 2023

Keywords:
Amyloid fibrils
Nanocellulose
Colloidal interactions
Self-assembly
Gelation

ABSTRACT

Amyloid fibrils from inexpensive food proteins and nanocellulose are renewable and biodegradable materials with broad ranging applications, such as water purification, bioplastics and biomaterials. To improve the mechanical properties of hybrid amyloid-nanocellulose materials, their colloidal interactions need to be understood and tuned. A combination of turbidity and zeta potential measurements, rheology and atomic force microscopy point to the importance of electrostatic interactions. These interactions lead to entropy-driven polyelectrolyte complexation for positively charged hen egg white lysozyme (HEWL) amyloids with negatively charged nanocellulose. The complexation increased the elasticity of the amyloid network by cross-linking individual fibrils. Scaling laws suggest different contributions to elasticity depending on nanocellulose morphology: cellulose nanocrystals induce amyloid bundling and network formation, while cellulose nanofibrils contribute to a second network. The contribution of the amyloids to the elasticity of the entire network structure is independent of nanocellulose morphology and agrees with theoretical scaling laws. Finally, strong and almost transparent hybrid amyloid-nanocellulose gels were prepared in a slow self-assembly started from repulsive co-dispersions above the isoelectric point of the amyloids, followed by dialysis to decrease the pH and induce amyloid-nanocellulose attraction and cross-linking. In summary, the gained knowledge on colloidal interactions provides an important basis for the design of functional biohybrid materials based on these two biopolymers.

1. Introduction

Amyloids are fibrillar protein aggregates with a characteristic structure consisting of antiparallel β-sheets stacked perpendicular to the fibril axis [1]. Albeit amyloids are notorious for their role in

* Corresponding authors at: Laboratory for Cellulose & Wood Materials, Empa – Swiss Federal Laboratories for Materials Science and Technology, Überlandstrasse 129, 8600 Dübendorf, Switzerland.
E-mail addresses: nico.kummer@empa.ch (N. Kummer), caroline.giacomin@hest.ethz.ch (C.E. Giacomin), peter.fischer@hest.ethz.ch (P. Fischer), silvia.campioni@empa.ch (S. Campioni), gustav.nystroem@empa.ch (G. Nyström).

https://doi.org/10.1016/j.jcis.2023.03.002
0021-9797/

many human diseases (e.g. Alzheimer's and Parkinson's), there are many known examples of functional amyloid fibrils, not only in microorganisms, but also in humans, where they are involved in hormone storage and release, and in the polymerization of melanin [2]. Some bacteria even exploit the rigidity and resistance to chemical or biological degradation of amyloid fibrils, which are a basic component of biofilms [2,3]. In addition to amyloid curli fibers, *Escherichia coli* biofilms also contain roughly 15% cellulose, resulting in a reinforced biocomposite, self-assembled into robust and elastic cage-like structures [4,5]. More generally, the rigidity and strength of amyloid fibrils makes them attractive for the design of renewable and biodegradable materials and simple aggregation protocols for the preparation of amyloids *in vitro* from inexpensive protein sources have been developed [2,6–9]. For instance, hen egg white lysozyme (HEWL) and milk β-lactoglobulin (BLG) are two food proteins that form amyloids after acid hydrolysis into peptide fragments, which in turn self-assemble into semi-flexible, high aspect ratio amyloid fibrils with the typical cross-β-sheet structure [10–13]. In recent years, amyloid fibrils made from HEWL and BLG in the form of hydrogels, aerogels, films and composites have found applications in biomaterials [2,9,14,15], membranes for water purification [16–19], bioplastics [20] and electronics [6].

To improve the mechanical properties of macroscopic amyloid materials, combinations of amyloid fibrils with polysaccharides [21] and with nanocelluloses [22,23] have been tested. Nanocelluloses are a class of bio-based and biodegradable materials with excellent mechanical properties and an immensely broad range of applications in functional materials [24–28]. The term "nanocelluloses" encompasses cellulose nanofibrils (CNFs) containing disordered and crystalline regions and pure crystalline cellulose nanocrystals (CNCs) [29,30]. Colloidally stable dispersions of CNFs can be obtained from wood pulp by oxidation with (2,2,6,6-tetramethylpiperidin-1-yl)oxyl (TEMPO) and mechanical grinding. The TEMPO-oxidized CNFs (TO-CNFs) are stabilized by negatively charged carboxyl groups [29]. CNCs are commonly prepared from wood pulp or cotton by a sulfuric acid hydrolysis treatment that shortens the CNCs and introduces negatively charged sulfate half-ester groups [30]. The negative charge of chemically modified nanocelluloses (or other polysaccharides) and the pH-dependent positive charge of proteins are the basis for polyelectrolyte complexation, a common type of interaction between oppositely charged polymers [28,31,32]. Polyelectrolytes are surrounded by an electrical double layer, a cloud of tightly packed counter-ions with reduced translational entropy. When complexes are formed through ionic bonds, the entropy of the polyelectrolytes is decreased, however the entropy of the system as a whole is increased due to the release of large amounts of counter-ions and bound water. Therefore, the driving force for complexation is the gain of entropy rather than short-ranged interactions between the polyelectrolytes [28,32–34]. In the specific case of positively charged, native lysozyme adsorbing onto mechanically disintegrated CNFs, isothermal titration calorimetry (ITC) proved that the adsorption is entropy-driven and influenced by the protonation state of hemicelluloses remaining on the CNF surface [35]. Similarly, the entropic gain from the release of water molecules and counter-ions and the strong effect of ionic interactions on the adsorption efficiency have been confirmed for negatively charged bovine serum albumin (BSA) mixed with positively charged pyridinium-grafted CNCs [36]. These purely physical interactions have been exploited to adsorb proteins onto nanocelluloses in order to prepare hybrid materials. Depending on the functionality of the protein (enzyme) possible applications include biocatalysis [37,38], sensing [39], and the use as antimicrobial material [40,41]. Composites of oppositely charged nanocellulose and HEWL amyloid fibrils have been studied in recent years. Positive HEWL amyloids possess a broad-spectrum antimicrobial activity [42] and have been used to prepare antimicrobial films, in combination with TO-CNF [43] and CNCs [22]. Combinations of HEWL amyloids and TO-CNF have also shown their potential for water purification, efficiently removing proteins, emulsion droplets and heavy metals [44,45]. However, the mechanical performance of hybrid amyloid-nanocellulose films and aerogels has been poor, as no synergistic effect has been observed so far [22,23,43]. The complexation of the oppositely charged polyelectrolyte particles seems to lead to inhomogeneity and to defects in the network, which adversely affect the overall mechanical performance [22,23,41].

To understand the interplay of these biocolloidal systems, we investigated the basic colloidal interactions in suspensions of HEWL and BLG amyloids with CNCs using turbidity measurements, zeta potential measurements, rheology and atomic force microscopy (AFM). Rheological measurements of the HEWL amyloid-CNC complexes were compared to those obtained using the unconverted peptide fraction. The dependence of the amyloid network elasticity on both amyloid and CNC concentration was tested and described with power laws. Finally, the self-assembly of amyloids with CNCs as cross-linkers was studied by co-dispersing the two components at a high pH at which both polymers are negatively charged, followed by dialysis against a low pH solution to introduce positive charges on the protein fibrils and thus induce their interaction and physical cross-linking with CNCs. This approach led to the formation of strong, almost transparent hybrid gels. To study the effect of nanocellulose morphology on the rheological properties of the hybrid gels, TO-CNFs were also considered in addition to the CNCs. Overall, the findings of this study contributes to an improved fundamental understanding of the colloidal interactions between amyloid fibrils and nanocellulose and provide important knowledge for the bottom-up self-assembly of functional biohybrid materials.

2. Experimental

2.1. Materials

HEWL (Mw = 14.3 kDa, purity > 90%) was purchased from Sigma-Aldrich. Purified BLG was (Mw = 18.4 kDa, purity > 97%) provided by the Food and Bioprocess Engineering group at the Technical University of Munich [46]. CNCs were purchased from CelluForce. TO-CNFs were prepared in-house according to a previously published protocol [41].

The 4-(2-hydroxyethyl)-1-piperazineethanesulfonic acid (HEPES, purity > 99.5%), sodium hydroxide (NaOH, purity > 99%) and hydrochloric acid (HCl, 37%) were obtained from VWR. The (3-aminopropyl)triethoxysilane (APTES, purity > 98%) was purchased from Sigma-Aldrich. All chemicals were used as received without further purification.

2.2. Methods

2.2.1. Preparation of amyloid fractions

HEWL and BLG amyloid fibrils were prepared by acid hydrolysis and aggregation at pH 2, 90 °C and protein concentrations of 2 wt% as described before [42]. After 24 h and 5 h for HEWL and BLG, respectively, semi-flexible, high aspect ratio amyloid fibrils were formed. In both cases, roughly 38% of the protein was converted into amyloid fibrils, while the rest of the protein occurs as hydrolyzed peptides [42,47]. Stiff amyloid fibrils a few hundred nanometers long were prepared using a probe sonicator [22,23,42]. The unconverted peptide fraction was separated from the amyloid fibrils using a centrifugal filter (Amicon) with a molecular weight cut-off (MWCO) of 100 kDa, and the exact concentration was measured by UV–Vis spectroscopy [42]. The suspensions of the different

amyloid fractions, from now on called amyloids, sonicated amyloids and peptides, were stored in the refrigerator at 4 °C until further use.

2.2.2. Preparation of nanocellulose suspensions

A stock CNC suspension was prepared at a concentration of 2 wt % by mixing the CNCs with MilliQ water using stirring and tip sonication (Digital Sonifier 450, Branson Ultrasonics) [22]. The concentration of the original TO-CNF suspension was 1.4 wt%.

2.2.3. Mixing of amyloid fractions and nanocellulose

The amyloid fractions and the nanocellulose stocks were diluted with 10 mM HEPES buffer at pH 7 to a final concentration of 2 mg/mL. The pH of the suspension was measured and adjusted to 7 with 1 M HCl or NaOH. Subsequently, the amyloid fractions and the nanocellulose were mixed in different ratios, keeping one component at a constant final concentration of 1 mg/mL (denoted by the index 10) and adding the other component at a final concentration of 0.1, 0.2, 0.3, 0.5, 0.7, 1.0, and 2.0 mg/mL (denoted by indices 1 to 20). An amyloid to nanocellulose ratio of 1 to 0.1 mg/mL would be denoted by 10:1, while a sample containing 0.1 mg/mL amyloids and 1 mg/mL nanocellulose would be denoted by 1:10. It should be noted, that the total solid content varied throughout a series of amyloid-nanocellulose ratios. A detailed mixing plan can be found in Table S1.

2.2.4. Optical characterization

The optical density of the mixed amyloid-CNC samples was measured at a wavelength of 600 nm using a Cary 1E spectrophotometer. The measurements were performed in PMMA cuvettes with a path length of 1 cm and the baseline measurement of 10 mM HEPES buffer at pH 7 was subtracted. Additionally, photographs of the suspensions were taken to show the increase in turbidity due to complexation.

2.2.5. ζ potential measurements

The different amyloids and nanocellulose ratios were diluted by a factor of 10, using 10 mM HEPES buffer at pH 7. The ζ potential measurements were performed in triplicate using a Malvern Zetasizer nano ZS equipped with a folded capillary cell. The mean and the standard deviation of the three measurements are reported. However, since standard deviations were in general very small, they were not visible in some of the figures.

2.2.6. Atomic force microscopy

The complexation of the different amyloid fractions with the CNCs in the nanometer range was studied by AFM imaging in tapping mode using a Bruker Icon 3 AFM equipped with Bruker RTESPA-150 probes. The samples were diluted by a factor of 10, using 10 mM HEPES buffer at pH 7 (pure CNCs were diluted to 0.01 mg/mL). After vortexing, 100 µL were dropped onto freshly cleaved mica, adsorbed for 1 min and then rinsed off with 1 mL MilliQ water. For the samples with positive zeta potentials, negatively charged unmodified mica was used, whereas for samples with negative zeta potentials, the mica was modified with APTES to make it positively charged. The images were acquired at a scan rate of 0.5 Hz and a resolution of 1024x1024 lines. The raw data was flattened and processed with the Bruker Nanoscope software.

2.2.7. Rheological characterization

The rheological properties of the amyloid-nanocellulose mixtures were measured with an Anton Paar MCR 702 rheometer equipped with a double gap geometry DG26.7. During the measurement the temperature of the samples was kept constant at 20 °C using a Peltier element. The linear viscoelastic regime was prescreened by amplitude sweeps at frequencies of 0.1, 1, and 10 rad/s. Finally, a frequency sweep from 0.1 to 100 rad/s at constant shear strain of 1 % and an amplitude sweep from 0.1 to 1000 % shear strain at a frequency of 1 rad/s were performed. Subsequently, the measuring cell was loaded with fresh sample and the shear viscosity was measured at shear rates ranging from 0.01 to 100 s^{-1}.

The dependence of the amyloid network elasticity on amyloid and nanocellulose concentration was characterized with the plateau storage modulus G_0 obtained from the storage modulus G' measured in the frequency sweeps at a fixed amplitude of 1 %. The mean of G_0 determined in triplicate, with error bars for the standard deviation was plotted against the amyloid and nanocellulose concentrations, respectively, in a double-logarithmic plot. The slope of the linear regression fitted with Origin 2022 (OriginLab Corporation, Northampton, MA, USA) including the standard deviation of the fit was taken as the exponent of the power law.

2.2.8. pH induced gelation

The HEWL and BLG amyloids were co-dispersed with the CNCs at a pH above the isoelectric point (pI) of the proteins, where both the amyloids and the CNCs are negatively charged. In order to immediately cross the pI during mixing, the 5 mL of 2 wt% HEWL amyloids at pH 2 were slowly mixed into 5 mL 2 wt% CNCs containing 75 µL 4 M NaOH. In the case of co-dispersions of BLG amyloids with CNCs, both components were brought to pH 7 and then mixed. The gelation of the mixtures was induced by lowering the pH below the pI of the protein, where the amyloids are positively charged and complexation with the CNCs leads to physical crosslinks. The pH change was achieved by using cut off 50 mL centrifuge tubes and covering the newly formed opening with a 1 kDa MWCO dialysis membrane (Repligen) attached with parafilm, similar to the setup described by Usuelli *et al.* [21]. For the rheological measurements, 2 mL of the CNC-amyloid co-dispersion were transferred into the custom-made dialysis tubes and then put into pH-adjusted (pH 3, 5, 7, 9) MilliQ baths overnight. The inner diameters of the dialysis tubes and the rough plate-plate geometry were both 25 mm, which enabled non-invasive (no cutting *et cetera*) analysis of the viscoelasticity of the gels. Frequency sweeps of the co-dispersions and the gels were measured at 1% deformation in the range of 0.1 to 1000 rad/s. Compression tests were performed using the Anton Paar MCR 702 multidrive rheometer equipped with linear motor and the rough plate-plate geometry.

2.2.9. Cryogenic scanning and transmission electron microscopy

Samples for cryo-SEM were prepared by placing 5 µL of the liquid samples (pure amyloid fibrils and CNCs) on carbon coated TEM-grids (Quantifoil, Germany) previously positively glow-discharged (Pelco easiGlow, TedPella, USA). For the hydrogel samples, the grid was placed onto the gel surface and then removed with material from inside the hydrogel exposed. After blotting and washing (for gel samples washing was omitted), the grids were plunge-frozen in a mix of liquid ethane/propane, freeze-dried up to –80 °C in a freeze-fracturing system BAF 060 (Bal-Tec/Leica, Vienna), then coated with tungsten (3 nm at an elevation angle of 45° and 3 nm at 90°) and imaged at −120 °C and 2 kV in a field emission SEM Leo Gemini 1530 (Zeiss, Germany) equipped with a cold stage (VCT Cryostage, Bal-Tec/Leica, Vienna). In-lens SE and Everhart-Thornley SE-signals at an acceleration voltage of 2 kV were used for image acquisition.

For cryo-TEM, aliquots of samples were applied onto lacey carbon-coated copper grids (EMS, USA), which were previously positively glow-discharged (Pelco easiGlow, TedPella, USA). Excess of sample was blotted away for two seconds and the grids were plunge frozen in a mixture of liquid ethane/propane (continuously cooled by liquid nitrogen) using a Vitrobot Mark IV (Thermo Fisher

Scientific, USA) with the environmental chamber set to 22 °C and 100% humidity. Vitrified grids were stored in liquid nitrogen until further processing. The cryo-EM grids were loaded into a Titan Krios microscope operating at 300 kV (Thermo Fisher Scientific, USA), equipped with a Gatan Quantum-LS Energy Filter (GIF) and a Gatan K2 Summit direct electron detector. The samples were imaged in EFTEM mode using the Thermo Fisher Scientific EPU software (81000x magnification, ca. 40 e/A2 total electron dose, K2 in linear mode), with a defocus range of −2 to −4 µm. The diameters of the amyloids, CNCs and structures formed in the hybrid amyloid-CNC gels were measured using ImageJ software [48]. In total, the diameters of 30 individual objects from several images were analyzed and reported as mean and standard deviation.

3. Results and discussion

3.1. Effect of charge on the interactions between amyloids and CNCs

To probe the colloidal interactions between amyloids and CNCs, mixed suspensions at different ratios (index 10 = 1 mg/mL) were prepared (Table S1). HEPES buffer (10 mM) was used to keep the pH constant at 7, at which HEWL amyloids were positively charged and BLG amyloids were negatively charged, respectively. Upon aggregation, both HEWL and BLG form semi-flexible amyloid fibrils with diameters of few nanometers and lengths of several micrometers, as shown by AFM (images on the left in Fig. 1). CNCs are stiff rod-like particles with diameters of a few nanometers and lengths of several hundred nanometers (image in the middle in Fig. 1). Upon mixing HEWL amyloids with CNCs at a ratio of 10:3, complexation was observed, while CNCs and BLG amyloid mixtures were homogenously co-dispersed (images on the right in Fig. 1). Note that, the AFM images should be taken as qualitative snapshots of the interactions (complexation vs. co-dispersion) occurring in the respective systems and cannot be compared in terms of amyloid or CNC concentrations. The complexation of HEWL amyloids with CNCs resulted in an increased turbidity, due to the increased scattering of light (turbidity measurements in Fig. 2**A** and photographs in Figure S1). In contrast, BLG amyloid-CNC co-dispersions remained transparent. Moreover, the complexation led to a compensation of the positive charge of the HEWL amyloids by the CNCs, as observed with ζ potential measurements (Fig. 2**B**). HEWL amyloids at pH 7 had a ζ potential of + 30 mV, which was decreased with increasing amounts of added CNCs (ζ potential −40 mV). The charge was completely neutralized at a HEWL amyloid-CNC ratio of 6:10 (zero net charge). The ζ potential values of BLG amyloids (-37 mV) and CNCs were almost identical, which explained the nearly constant slope over all the measured ratios. It should be pointed out that the peak in turbidity was shifted to a ratio of 10:10 for the HEWL amyloid-CNC system and instead of the point of zero net charge (6:10). This can be attributed to the increased total solid content at the 10:10 ratio forming more complexes that scatter light and cause turbidity. Furthermore, the complexation of HEWL amyloids and CNCs led to an increase of the viscoelastic properties of the amyloid network, while the storage modulus G' and loss modulus G'' remained low for the CNC-BLG amyloid co-dispersions (Fig. 2**C**). The same complexation behavior upon mixing with CNCs was found for shortened amyloid fibrils and unconverted peptides (Figure S2 and S3), with reduced rheological properties compared to full-length amyloids (Figure S4).

Overall the results in Fig. 1 and Fig. 2 demonstrate the importance of ionic interactions in promoting the complexation between protein amyloids and CNCs. As already pointed out by several studies of our group, polyelectrolyte complexation dominates the interactions of both native (i.e. monomeric) HEWL and HEWL amyloids with nanocelluloses [22,23,41]. The oppositely charged HEWL amyloids mixed with CNCs undergo complexation driven by the gain of entropy in the system, due to the release of counter-ions and bound water, rather than short-ranged ionic interactions [35,36]. Already the pure amyloid suspensions (10:0) formed a network of semi-flexible fibrils, as shown in the rheology measurements (G' > G''). The increase of G' upon the addition of CNCs, while keeping the HEWL amyloid concentration constant (10:10), suggested the formation of cross-links in the amyloid network.

3.2. Origin of the amyloid network elasticity

Rheology measurements also indicated that the viscoelastic properties of a network of HEWL amyloids and CNCs strongly depend on the ratio between these two particles, as this is related to the degree of complexation and cross-linking (Fig. 3). The

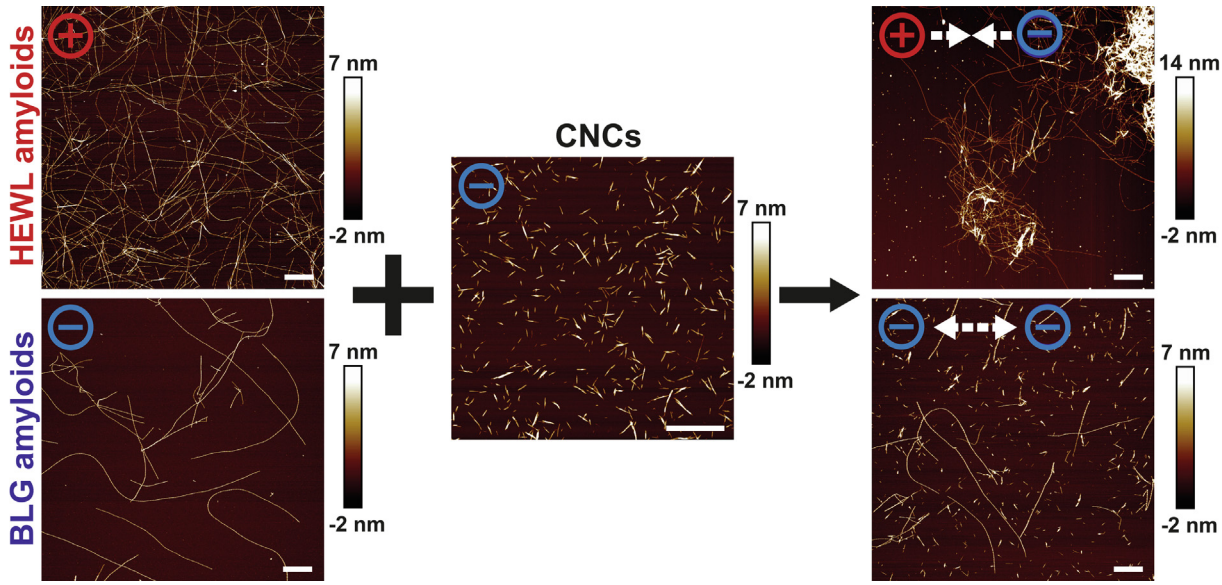

Fig. 1. AFM images of HEWL and BLG amyloid fibrils and their mixtures with CNCs at an amyloids:CNC ratio of 10:3. The scale bars correspond to 1 µm.

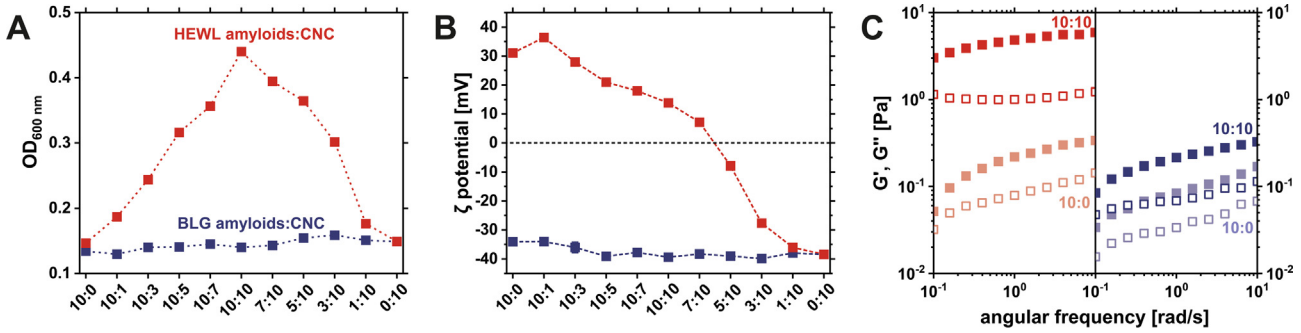

Fig. 2. Turbidity (OD_{600}) (A) and ζ potential measurements (B) of amyloid-CNC mixtures at different ratios. Frequency sweeps at a fixed amplitude of 1% of pure HEWL and BLG amyloid fibrils (10:0) and amyloid-CNC mixtures at the 10:10 ratio, 10 = 1 mg/mL (C).

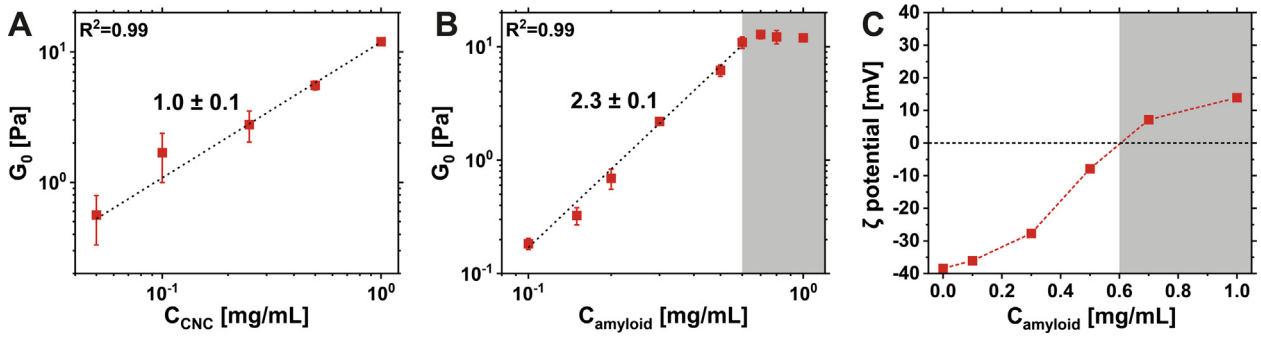

Fig. 3. The plateau modulus G_0 at a fixed amyloid concentration of 1 mg/mL in dependence on the added CNCs, including the linear fit determining the exponent of the power law (A). The plateau modulus G_0 at a fixed CNC concentration of 1 mg/mL in dependence on the amyloid concentration, including the linear fit determining the exponent of the power law for concentrations up to 0.6 mg/mL (white regime) (B). At higher concentrations a plateau was reached (grey regime). The ζ potentials at a fixed CNC concentration of 1 mg/mL with increasing amyloid additions at pH 7 (C).

frequency sweeps of samples at a fixed amyloid concentration (10 = 1 mg/mL) and increasing amounts of CNCs indicated a progressive increase of G' values. Plotting the plateau modulus G_0 (G' at 1% amplitude and 1 rad/s frequency) against the concentration of CNCs/amyloids, in a double-logarithmic plot, while keeping the respective other component constant, allowed to determine power laws (Fig. 3A and 3B). The scaling behaviours of $G_0 \sim c_{CNC}^{1.0\pm0.1}$ and $G_0 \sim c_{amyloids}^{2.3\pm0.1}$ were found. The power law for the amyloid concentration dependence was only valid for HEWL amyloid concentrations up to 0.6 mg/mL (white regime), while a plateau was reached at higher amounts of amyloids (grey regime). At this CNC-amyloid ratio of 6:10, all the CNCs (fixed concentration of 10 = 1 mg/mL) were assumed to be adsorbed onto the amyloid fibrils and their ability to further cross-link the amyloid network was exhausted. Therefore, higher additions of amyloids were not efficiently cross-linked and no further increase in elasticity was observed in the considered concentration window. This finding was supported by the zero net charge between the 5:10 and 7:10 ratio, as determined by ζ potential measurements (Fig. 2B). This corresponds to an amyloid concentration of roughly 0.6 mg/mL, as shown also in Fig. 3C, were the ζ potentials were replotted against the concentration of amyloids. The same set of experiments was also performed for BLG amyloids mixed with CNCs at pH 3, with similar results ($G_0 \sim c_{CNC}^{1.4\pm0.1}$ and $G_0 \sim c_{amyloids}^{2.3\pm0.4}$), however only four data points could be used for fitting, since the plateau was reached already at 0.3 mg/mL BLG amyloid concentration (Figure S5).

The determined power laws allow to draw certain conclusions about the structure of the network and the reason for its elasticity. The power law $G_0 \sim c_{CNC}^{1.0\pm0.1}$ reflects an almost proportional response of the elasticity when more CNCs are added. This lack of a synergistic effect on the mechanical properties of hybrid amyloid-nanocellulose films and aerogels has been observed before and was attributed to inhomogenities causing defects in the network [22,23]. The exponent of the power law can provide information about the cross-linking mechanism. For instance, a much higher exponent of 4.4 was obtained for BLG and HEWL amyloid networks cross-linked with sodium chloride (NaCl), suggesting a cross-linking mechanism based on charge screening, which effectively increased the probability for physical cross-links to form at the entanglement points in the network [49]. Further examples for exponents larger than 1 are associated with the bundle formation (increase of the bending rigidity of the building blocks of the network) of actin filaments induced by the specific binding of scruin or fascin proteins (exponents of 2 and 1.5, respectively) [50,51]. Instead, a lower exponent of 0.6 has been reported for intermediate filaments, due to the cross-linking with Ca^{2+} ions occurring via negatively charged side chains. Here, the cross-linking efficiency was reduced due to cross-links forming between side chains of the same filament, which then did not contribute to the elasticity of the intermediate filament network [52]. Based on these literature examples, we hypothesize that the cross-linking occurs through a mixed process of cross-linking at entanglement points, amyloid bundling and CNC aggregation with residual unconverted peptides (roughly 60% of the total protein mass [42]), effectively reducing the CNC surface available for cross-linking with amyloids and thus the contribution to the network elasticity.

The scaling of the elasticity with amyloid concentration to the power of 2.3 ± 0.1 is in good agreement with theoretical models and experimental data for semi-flexible polymers [53,54]. Mackintosh *et al.* [54] developed the affine thermal model to describe the elasticity of actin networks:

$$G_0 \sim \frac{\kappa^2}{k_B T} \xi^{-2} L_e^{-3}$$

where κ denotes the bending modulus, k_B the Boltzmann constant, T the absolute temperature, ξ the average mesh size of the network, and L_e the characteristic entanglement length. Since $\xi \sim c_{amyloid}^{-1/2}$ and $L_e \sim c_{amyloid}^{-2/5}$ the elasticity scales with the amyloid concentration to the power of 2.2 [53]:

$$G_0 \sim c_{amyloid}^{11/5}$$

Indeed, Cao *et al.* found exponents of 2.2 for semiflexible BLG and HEWL amyloids cross-linked with NaCl, fitting the affine thermal model [49]. Instead, van Dalen *et al.* used the non-affine floppy modes model on to describe their HEWL amyloid network elasticity, scaling with the amyloid concentration to the power of 2.4 [55].

3.3. Using pH-dependent charge of amyloids to induce gelation

With the gained knowledge on amyloid-CNC interactions, hybrid gels at a total solid content of 20 mg/mL were self-assembled exploiting the dependence of the charge of the amyloids on the pH (Fig. 4**A and 4B**). To have a purely repulsive system where both particles are co-dispersed in absence of complexation, amyloids and CNCs were homogenously mixed at a pH higher than the isoelectric point (10.2 in the case of HEWL amyloids and 5.2 for BLG amyloids) (Fig. 4**C**). The co-dispersions were pipetted into a custom-made dialysis tube, which was immersed into MilliQ water at pH 7 (for HEWL amyloid-CNC mixtures) or pH 3 (for BLG amyloid-CNC mixtures), respectively. This pH shift to a value lower than the isoelectric point of the amyloids introduced positive charges on the protein colloids, enabling ionic interactions with the negatively charged CNCs (Fig. 4**D**, data for dispersions at amyloid-CNC 10:10). After overnight dialysis, homogenous and almost transparent amyloid-CNC hybrid gels were formed with both HEWL amyloids (Fig. 4B red frame) and BLG amyloids (Fig. 4B blue frame). The HEWL amyloid-CNC gels trapped some air bubbles, which was the reason for the seemingly lower transparency. Overall, the slow self-assembly of the hybrid network led to homogenous gels and the formation of light-scattering features could be avoided. Fig. 4**E** shows the increased storage modulus of the gels compared to the co-dispersions (1.5 and 2.5 orders of magnitude for HEWL amyloid-CNC and BLG amyloid-CNC gels, respectively). The higher storage modulus of the CNC-HEWL amyloid co-dispersion compared to the CNC-BLG amyloid co-dispersion was due to the addition of the sodium hydroxide needed to reach pH 12 (roughly 30 mM), which led to charge screening by Na^+ and slight aggregation of the CNCs [56]. The storage moduli of both gels reached several kPa, which is slightly higher than previous values measured for amyloid gels at the same total solid content (20 mg/mL) cross-linked with 300 mM NaCl and reinforced with different polysaccharides [21]. Fig. 4**F** shows the dependence of G_0 on the equilibrium pH after dialysis for HEWL amyloid-CNC gels. As seen before, the 1.5 order of magnitude increase in G_0 occurred after crossing the isoelectric point. The elasticity gradually increased when the pH was lowered, from ~ 3000 Pa at pH 9 to ~ 8000 Pa at pH 3. This can be associated to the increased linear charge density of the HEWL amyloids (ζ potential in Fig. 4C) at lower pH, and to the ability to form more or stronger cross-links with CNCs.

Cryo-SEM imaging was performed on gels containing 10 mg/mL HEWL amyloids and 5 mg/mL CNCs to understand the structure of the self-assembled hybrid hydrogels (Fig. 5). Predominantly, lateral aggregation of amyloid fibrils and CNCs into bundles was observed. Detailed analysis of the diameter of pure HEWL amyloids and CNCs, as well as the formed bundles, proved that the bundles were on average three times as wide as the single components. To confirm that the bundles were not an artifact formed during the freeze-drying prior the cryo-SEM imaging, vitrified and still hydrated samples were imaged using cryo-TEM (Figure S6).

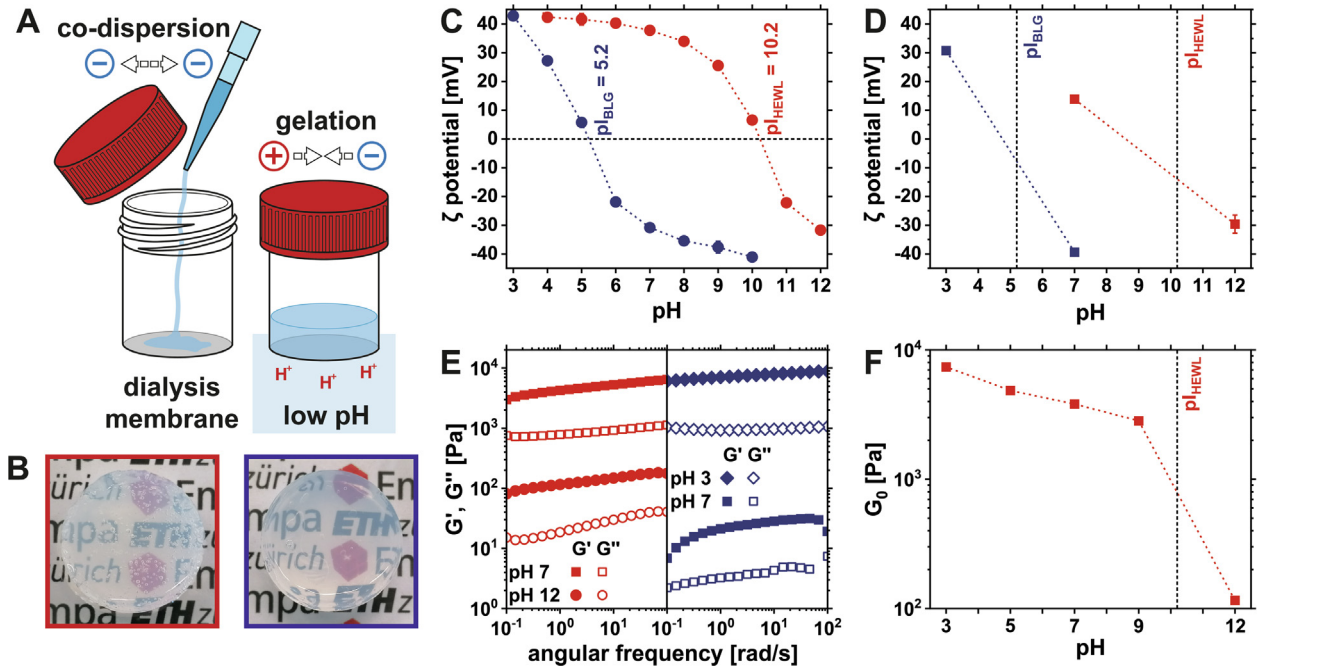

Fig. 4. Illustration of the slow pH-mediated self-assembly of amyloids and CNCs (A). Photographs of hybrid amyloid-CNC gels (red. HEWL, blue. BLG) at a concentration of 10 mg/mL amyloids and CNCs each (B). pH-dependent ζ potentials of pure HEWL and BLG amyloids including isoelectric points (C). ζ potential measurements of the amyloid-CNC mixtures (10:10 ratio) at different pH. The data points were connected by a line to guide the eye (D). Frequency sweeps of the amyloid-CNC hybrid gels and the co-dispersions at the corresponding pH (E). pH-dependent plateau storage modulus G_0 (F). (For interpretation of the references to colour in this figure legend, the reader is referred to the web version of this article.)

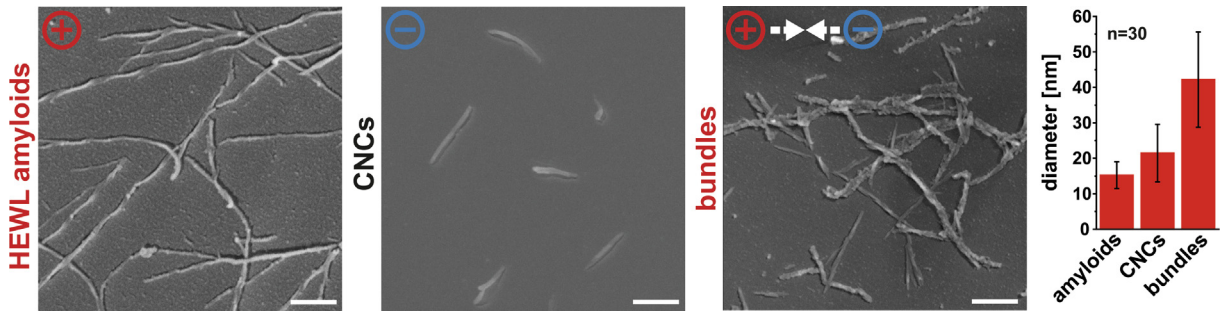

Fig. 5. Cryo-SEM images of HEWL amyloid and CNC suspensions, as well as amyloid-CNC bundles found in hybrid gels. The diameter of the bundles increased by a factor of three compared to pure amyloids and CNCs. The scale bars correspond to 100 nm.

As already mentioned above, bundling is a common mechanisms in protein filament networks [50,51] and the exponents found in the scaling laws (Fig. 3A and S5A) indicate that addition of CNCs induces cross-linking of amyloids through bundling. In the case of positive HEWL amyloids and oppositely charged CNCs the rules of entropy-driven polyelectrolyte complexation apply [31,32]. Therefore, lateral aggregation is favored since it leads to the minimization of free surface area of these rod-like particles, maximizing the release of hydration water and counter-ions and therefore the entropy in the system.

3.4. HEWL amyloid-TO-CNF system

With the knowledge on the interactions and self-assembly of amyloids with CNCs at hand, mixtures of HEWL amyloids and TO-CNF were also investigated by rheology to assess their complexation behavior. Scaling laws of the plateau modulus G_0 (G' at 1% amplitude and 1 rad/s frequency) with HEWL amyloids and TO-CNF concentrations were measured (Fig. 6**A and 6B**). Due to the robustness of the method demonstrated above, a single measurement series was sufficient to get reliable data. The scaling behaviours of $G_0 \sim c_{TO-CNF}^{4.0\pm0.2}$ and $G_0 \sim c_{amyloids}^{2.4\pm0.1}$ were found.

The power law for the TO-CNF concentration dependence was only valid for concentrations up to 0.3 mg/mL (white regime), while a plateau was reached at higher amounts of TO-CNF (grey regime). At this ratio of TO-CNF and HEWL amyloids of 10:3, the positve charge of the amyloids (fixed concentration of 10 = 1 mg/mL) in the system is fully compensated by TO-CNFs and any further addition of TO-CNFs would not lead to more cross-linking and increased elasticity. Zeta potential measurements show that the net zero charge of the system is found at around this ratio (Fig. 6**C**).

As for the amyloid-CNC system scaling laws were successfully fitted and linked to the charge-dependent cross-linking between amyloids and nanocellulose. The almost identical exponent of 2.4 for the scaling law with amyloid concentration agrees well with both theory and experimental data [49,53–55], describing the contribution of the amyloid fibrils to network elasticity. On the other hand, the elasticity scaling with TO-CNFs was fundamentally different to the scaling with CNCs. The much higher exponent of 4.0 can be explained by the fact that the TO–CNF efficiently contribute to the elasticity of the system by forming a network. While CNCs are not able to form a network at the concentrations added in the experiment, the overlap concentration of TO-CNFs is in a concentration window where the formation of TO-CNF networks has been previously reported [28,57]. The exponent of 4.0 ± 0.1 lies in between theoretical exponents of 3.67 for the relevant concentration range [58] and experimental scaling exponents for TO-CNFs of 4.1 and 4.5, respectively [59,60].

To test if the additional TO-CNF network improved the strength of the self-assembled hybrid gels made with the pH-switch method (Fig. 4A), amyloid-CNC and amyloid-CNF gels containing 10 mg/mL amyloids and 7 mg/mL nanocellulose were prepared. The mechanical performance of the hybrid gels was tested with oscillatory shear rheology and oscillatory compression testing (Fig. 7). The pH-mediated gelation increased the oscillatory shear moduli of the amyloid-nanocellulose mixtures by almost two orders of magnitude (Fig. 7A). The nanocellulose morphology did not have an effect on the G' values, as no difference was seen between hybrid gels containing CNCs or TO-CNF. However, the strain of the dynamic yield point (indicated by arrows in Fig. 7B) increased by almost an order of magnitude in hybrid gels containing TO-CNF. Finally, compression testing (Fig. 7C) showed no difference in elongational elastic modulus E' in the linear regime.

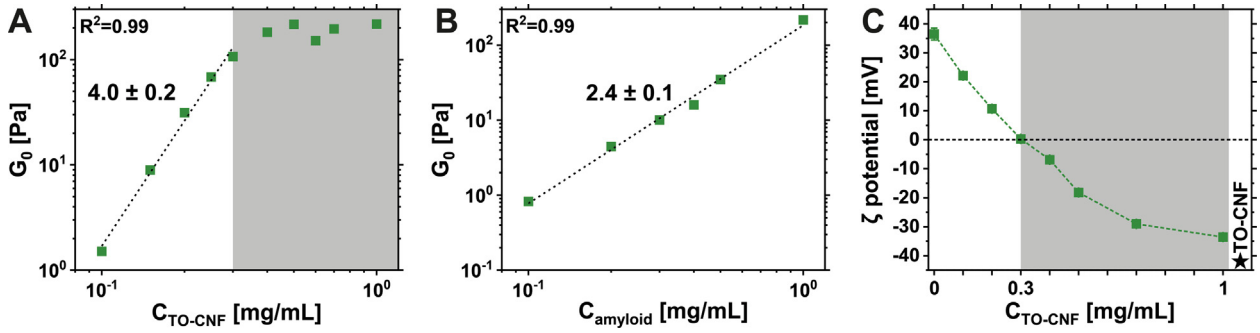

Fig. 6. The plateau modulus G_0 at a fixed HEWL amyloid concentration of 1 mg/mL in dependence on the added TO-CNFs, including the linear fit determining the exponent of the power law for concentrations up to 0.3 mg/mL (white regime) (A). At higher concentrations a plateau was reached (grey regime). The plateau modulus G_0 at a fixed TO-CNF concentration of 1 mg/mL in dependence on the amyloid concentration, including the linear fit determining the exponent of the power (B). The ζ potentials at a fixed HEWL amyloid concentration of 1 mg/mL with increasing TO-CNF additions at pH 7 (C).

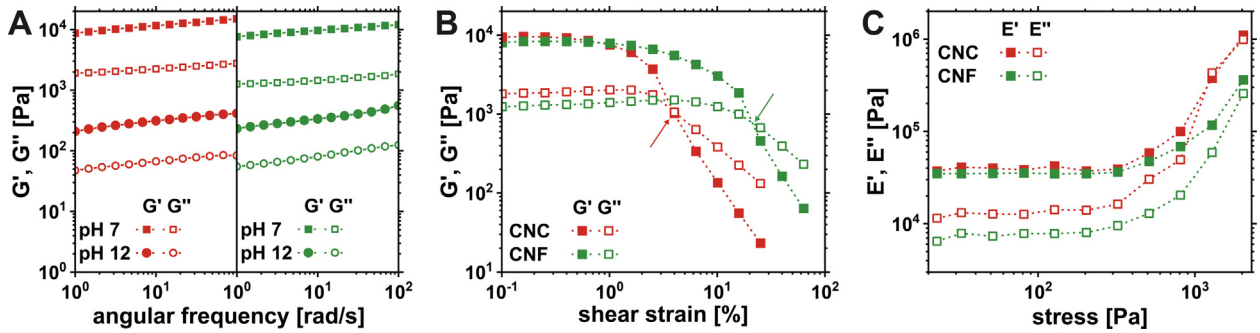

Fig. 7. Frequency sweeps of the amyloid-nanocellulose (CNCs in red, TO-CNFs in green) hybrid gels and the co-dispersions at the corresponding pH (A), amplitude sweeps of the hybrid gels at a fixed frequency of 1 rad/s, with arrows indicating the dynamic yield points (B), and oscillatory compression testing of the hybrid gels (C). (For interpretation of the references to colour in this figure legend, the reader is referred to the web version of this article.)

The expected strengthening of the hybrid gels by switching from CNCs to TO-CNFs was rather challenging to observe in the mechanical experiments presented here. Although the gels amyloid-CNF gels were visibly more durable during sample handling, there was no difference in the linear regimes during frequency sweeps in shear rheology and in compression testing. Only the amplitude sweep data showed that the amyloid-CNF gels can withstand larger deformations. This can be attributed to the presence of two networks, increasing the overall toughness of the material. This set of experiments would be greatly improved with tensile measurements as shear and compression do not seem to be the ideal type of deformation to gain more knowledge on their mechanical properties. Unfortunately, these gels are not stable enough to be mounted into a tensile geometry.

4. Conclusion

The interactions between amyloid fibrils and nanocellulose were largely dependent on charge: AFM imaging, turbidity measurements, zeta potential measurements and rheology proved the attraction of positively charged HEWL amyloids and oppositely charged CNCs, while negatively charged BLG amyloids and CNCs repulsed each other and formed stable co-dispersions. The polyelectrolyte complexation of HEWL amyloids and nanocellulose is driven by the gain of entropy in the system due to the release of counter-ions and hydration water. The emerging complexes can be considered as HEWL amyloid networks cross-linked with nanocellulose. In-depth rheological characterization allowed description of the amyloid network elasticity as a function of amyloid and nanocellulose concentration. While the $G_0 \sim c_{CNC}^{1.0\pm0.1}$ relationship shows the proportional increase of elasticity with CNC addition, attributed to cross-link formation and bundling, the $G_0 \sim c_{CNF}^{4.0\pm0.1}$ scaling law indicates the formation of a double network of the added TO-CNFs [58–60]. On the other hand, the scaling of elasticity with amyloid concentration to the exponent of 2.3 ± 0.1 is in good agreement with the affine thermal model and experimental data for amyloid fibrils and other filamentous proteins [49,53–55]. Finally, homogenous, almost transparent hybrid HEWL and BLG amyloid-nanocellulose gels were made using a pH-mediated self-assembly method. In order to go from a repulsive co-dispersion of negative amyloids and nanocellulose, the pI was crossed, introducing positive charges on the amyloid and leading to a nanocellulose-amyloid network. The nanocellulose morphology did not affect the elastic modulus in shear and compression measurements, but the hybrid gels containing TO-CNF showed a higher dynamic yield point, and can therefore withstand larger deformations. Due to their higher aspect ratio and thus lower overlap concentration, the addition of TO-CNF will contribute an additional network and therefore, amyloid-CNF hybrid materials have better mechanical properties compared to amyloid-CNC hybrids. In conclusion, these results contribute to the understanding of amyloid-nanocellulose interactions and self-assembly, and provide strategies for future work on the bottom-up assembly of sustainable hybrid functional materials.

CRediT authorship contribution statement

Nico Kummer: Conceptualization, Data curation, Formal analysis, Investigation, Methodology, Project administration, Validation, Visualization, Writing – original draft. **Caroline E. Giacomin:** Formal analysis, Investigation, Methodology, Validation, Writing – review & editing. **Peter Fischer:** Conceptualization, Funding acquisition, Methodology, Supervision, Writing – review & editing. **Silvia Campioni:** Conceptualization, Funding acquisition, Project administration, Supervision, Writing – review & editing. **Gustav Nyström:** Conceptualization, Funding acquisition, Project administration, Supervision, Writing – review & editing.

Data availability

Data will be made available on request.

Declaration of Competing Interest

The authors declare that they have no known competing financial interests or personal relationships that could have appeared to influence the work reported in this paper.

Acknowledgements

The authors would like to thank Brian Sinnet for providing access to the Zetasizer at the Particle Laboratory of Eawag, Gilberto Siqueira (Empa) for providing the TO-CNF and Qiyao Sun for support with compression testing. Stephan Handschin and Miroslav Peterek from ScopEM at ETH are acknowledged for their support with cryo-EM. Kevin De France (Empa) and Mattia Usuelli (ETH Zurich) are acknowledged for valuable discussions. N. Kummer, S. Campioni and G. Nyström would like to gratefully acknowledge financial support from the Swiss National Science Foundation (Grant number: 200021_192225). C.E. Giacomin and P. Fischer acknowledge financial support from the Swiss National Science Foundation (Grant number: CRSII5_189917).

Appendix A. Supplementary data

Supplementary data to this article can be found online at https://doi.org/10.1016/j.jcis.2023.03.002.

References

[1] D.S. Eisenberg, M.R. Sawaya, Structural Studies of Amyloid Proteins at the Molecular Level, Annu. Rev. Biochem. 86 (2017) 69–95, https://doi.org/10.1146/annurev-biochem-061516-045104.

[2] T.P.J. Knowles, R. Mezzenga, Amyloid Fibrils as Building Blocks for Natural and Artificial Functional Materials, Adv. Mater. 28 (2016) 6546–6561, https://doi.org/10.1002/adma.201505961.

[3] M.M. Barnhart, M.R. Chapman, Curli Biogenesis and Function, Annu. Rev. Microbiol. 60 (2010) 131–147, https://doi.org/10.1146/annurev.micro.60.080805.142106.

[4] O.A. McCrate, X. Zhou, C. Reichhardt, L. Cegelski, Sum of the parts: Composition and architecture of the bacterial extracellular matrix, J. Mol. Biol. 425 (2013) 4286–4294, https://doi.org/10.1016/j.jmb.2013.06.022.

[5] W. Thongsomboon, D.O. Serra, A. Possling, C. Hadjineophytou, R. Hengge, L. Cegelski, Phosphoethanolamine cellulose: A naturally produced chemically modified cellulose, 359 (2018) 334–338. https://doi.org/https://doi.org/10.1126/science.aao4096.

[6] G. Wei, Z. Su, N.P. Reynolds, P. Arosio, I.W. Hamley, E. Gazit, R. Mezzenga, Self-assembling peptide and protein amyloids: From structure to tailored function in nanotechnology, Chem. Soc. Rev. 46 (2017) 4661–4708, https://doi.org/10.1039/c6cs00542j.

[7] Y. Cao, R. Mezzenga, Food protein amyloid fibrils: Origin, structure, formation, characterization, applications and health implications, Adv. Colloid Interface Sci. 269 (2019) 334–356, https://doi.org/10.1016/j.cis.2019.05.002.

[8] P.C. Ke, R. Zhou, L.C. Serpell, R. Riek, T.P.J. Knowles, H.A. Lashuel, E. Gazit, I.W. Hamley, T.P. Davis, M. Fändrich, D.E. Otzen, M.R. Chapman, C.M. Dobson, D.S. Eisenberg, R. Mezzenga, Half a century of amyloids: Past, present and future, Chem. Soc. Rev. 49 (2020) 5473–5509, https://doi.org/10.1039/c9cs00199a.

[9] Y. Shen, A. Levin, A. Kamada, Z. Toprakcioglu, M. Rodriguez-Garcia, Y. Xu, T.P.J. Knowles, From Protein Building Blocks to Functional Materials, ACS Nano. 15 (2021) 5819–5837, https://doi.org/10.1021/acsnano.0c08510.

[10] C. Lara, J. Adamcik, S. Jordens, R. Mezzenga, General self-assembly mechanism converting hydrolyzed globular proteins into giant multistranded amyloid ribbons, Biomacromolecules. 12 (2011) 1868–1875, https://doi.org/10.1021/bm200216u.

[11] E. Frare, P. Polverino De Laureto, J. Zurdo, C.M. Dobson, A. Fontana, A highly amyloidogenic region of hen lysozyme, J. Mol. Biol. 340 (2004) 1153–1165, https://doi.org/10.1016/j.jmb.2004.05.056.

[12] C. Veerman, H. Ruis, L.M.C. Sagis, E. van der Linden, Effect of electrostatic interactions on the percolation concentration of fibrillar β-lactoglobulin gels, Biomacromolecules. 3 (2002) 869–873, https://doi.org/10.1021/bm025533+.

[13] J.-M. Jung, D.Z. Gunes, R. Mezzenga, Interfacial Activity and Interfacial Shear Rheology of Native β-Lactoglobulin Monomers and Their Heat-Induced Fibers, Langmuir. 26 (2010) 15366–15375, https://doi.org/10.1021/la102721m.

[14] C. Li, A.K. Born, T. Schweizer, M. Zenobi-Wong, M. Cerruti, R. Mezzenga, Amyloid-hydroxyapatite bone biomimetic composites, Adv. Mater. 26 (2014) 3207–3212, https://doi.org/10.1002/adma.201306198.

[15] C. Li, R. Qin, R. Liu, S. Miao, P. Yang, Functional amyloid materials at surfaces/interfaces, Biomater. Sci. 6 (2018) 462–472, https://doi.org/10.1039/c7bm01124e.

[16] S. Bolisetty, R. Mezzenga, Amyloid-carbon hybrid membranes for universal water purification, Nat. Nanotechnol. 11 (2016) 365–371, https://doi.org/10.1038/nnano.2015.310.

[17] F. Yang, Z. Yan, J. Zhao, S. Miao, D. Wang, P. Yang, Rapid capture of trace precious metals by amyloid- like protein membrane with high adsorption capacity and selectivity (2020), https://doi.org/10.1039/C9TA12124B.

[18] M. Peydayesh, R. Mezzenga, Protein nanofibrils for next generation sustainable water purification, Nat. Commun. 12 (2021) 1–17, https://doi.org/10.1038/s41467-021-23388-2.

[19] M. Peydayesh, T. Suta, M. Usuelli, S. Handschin, G. Canelli, M. Bagnani, R. Mezzenga, Sustainable Removal of Microplastics and Natural Organic Matter from Water by Coagulation-Flocculation with Protein Amyloid Fibrils, Environ. Sci. Technol. 55 (2021) 8848–8858, https://doi.org/10.1021/acs.est.1c01918.

[20] M. Peydayesh, M. Bagnani, R. Mezzenga, Sustainable bioplastics from amyloid fibril-biodegradable polymer blends, ACS Sustain. Chem. Eng. 9 (2021) 11916–11926, https://doi.org/10.1021/acssuschemeng.1c03937.

[21] M. Usuelli, T. Germerdonk, Y. Cao, M. Peydayesh, M. Bagnani, S. Handschin, G. Nyström, R. Mezzenga, Polysaccharide-reinforced amyloid fibril hydrogels and aerogels, Nanoscale. 13 (2021) 12534–12545, https://doi.org/10.1039/d1nr03133c.

[22] K.J. De France, N. Kummer, Q. Ren, S. Campioni, G. Nyström, Assembly of Cellulose Nanocrystal-Lysozyme Composite Films with Varied Lysozyme Morphology, Biomacromolecules. 21 (2020) 5139–5147, https://doi.org/10.1021/acs.biomac.0c01267.

[23] L. Severini, K.J. De France, D. Sivaraman, N. Kummer, G. Nyström, Biohybrid Nanocellulose-Lysozyme Amyloid Aerogels via Electrostatic Complexation, ACS Omega. 7 (2022) 578–586, https://doi.org/10.1021/acsomega.1c05069.

[24] K.J. De France, T. Hoare, E.D. Cranston, Review of Hydrogels and Aerogels Containing Nanocellulose, Chem. Mater. 29 (2017) 4609–4631, https://doi.org/10.1021/acs.chemmater.7b00531.

[25] E. Kontturi, P. Laaksonen, M.B. Linder, A.H. Nonappa, O.J. Gröschel, O.I. Rojas, Advanced Materials through Assembly of Nanocelluloses, Adv. Mater. 30 (2018), https://doi.org/10.1002/adma.201703779.

[26] P. Bertsch, P. Fischer, Adsorption and interfacial structure of nanocelluloses at fluid interfaces, Adv. Colloid Interface Sci. 276 (2020), https://doi.org/10.1016/j.cis.2019.102089 102089.

[27] E. Niinivaara, E.D. Cranston, Bottom-up assembly of nanocellulose structures, Carbohydr. Polym. 247 (2020), https://doi.org/10.1016/j.carbpol.2020.116664 116664.

[28] T. Benselfelt, N. Kummer, M. Nordenström, A. Fall, G. Nyström, L. Wågberg, The Colloidal Properties of Nanocellulose, ChemSusChem (Accepted Author Manuscript). (2023). https://chemistry-europe.onlinelibrary.wiley.com/doi/10.1002/cssc.202201955.

[29] T. Saito, S. Kimura, Y. Nishiyama, A. Isogai, Cellulose nanofibers prepared by TEMPO-mediated oxidation of native cellulose, Biomacromolecules. 8 (2007) 2485–2491, https://doi.org/10.1021/bm0703970.

[30] S. Beck-Candanedo, M. Roman, D.G. Gray, Effect of reaction conditions on the properties and behavior of wood cellulose nanocrystal suspensions, Biomacromolecules. 6 (2005) 1048–1054, https://doi.org/10.1021/bm049300p.

[31] S.L. Turgeon, C. Schmitt, C. Sanchez, Protein-polysaccharide complexes and coacervates, Curr. Opin. Colloid Interface Sci. 12 (2007) 166–178, https://doi.org/10.1016/j.cocis.2007.07.007.

[32] J. van der Gucht, E. Spruijt, M. Lemmers, M.A. Cohen Stuart, Polyelectrolyte complexes: Bulk phases and colloidal systems, J. Colloid Interface Sci. 361 (2011) 407–422, https://doi.org/10.1016/j.jcis.2011.05.080.

[33] J. Gummel, F. Cousin, F. Boué, Counterions release from electrostatic complexes of polyelectrolytes and proteins of opposite charge: A direct measurement, J. Am. Chem. Soc. 129 (2007) 5806–5807, https://doi.org/10.1021/ja070414t.

[34] S. Lombardo, W. Thielemans, Thermodynamics of adsorption on nanocellulose surfaces, Cellulose. 26 (2019) 249–279, https://doi.org/10.1007/s10570-018-02239-2.

[35] R. Kolakovic, L. Peltonen, A. Laukkanen, M. Hellman, P. Laaksonen, M.B. Linder, J. Hirvonen, T. Laaksonen, Evaluation of drug interactions with nanofibrillar cellulose, Eur. J. Pharm. Biopharm. 85 (2013) 1238–1244, https://doi.org/10.1016/j.ejpb.2013.05.015.

[36] S. Lombardo, S. Eyley, C. Schütz, H. Van Gorp, S. Rosenfeldt, G. Van Den Mooter, W. Thielemans, Thermodynamic Study of the Interaction of Bovine Serum Albumin and Amino Acids with Cellulose Nanocrystals, Langmuir. 33 (2017) 5473–5481, https://doi.org/10.1021/acs.langmuir.7b00710.

[37] R. Weishaupt, G. Siqueira, M. Schubert, P. Tingaut, K. Maniura-Weber, T. Zimmermann, L. Thöny-Meyer, G. Faccio, J. Ihssen, TEMPO-Oxidized Nanofibrillated Cellulose as a High Density Carrier for Bioactive Molecules, Biomacromolecules. 16 (2015) 3640–3650, https://doi.org/10.1021/acs.biomac.5b01100.

[38] T. Nikolic, M. Korica, J. Milanovic, A. Kramar, Z. Petronijevic, M. Kostic, TEMPO-oxidized cotton as a substrate for trypsin immobilization: impact of functional groups on proteolytic activity and stability, Cellulose. 24 (2017) 1863–1875, https://doi.org/10.1007/s10570-017-1221-1.

[39] R. Weishaupt, G. Siqueira, M. Schubert, M.M. Kämpf, T. Zimmermann, K. Maniura-Weber, G. Faccio, A Protein-Nanocellulose Paper for Sensing Copper Ions at the Nano- to Micromolar Level, Adv. Funct. Mater. 27 (2017), https://doi.org/10.1002/adfm.201604291.

[40] R. Weishaupt, L. Heuberger, G. Siqueira, B. Gutt, T. Zimmermann, K. Maniura-Weber, S. Salentinig, G. Faccio, Enhanced Antimicrobial Activity and Structural Transitions of a Nanofibrillated Cellulose-Nisin Biocomposite Suspension, ACS Appl. Mater. Interfaces. 10 (2018) 20170–20181, https://doi.org/10.1021/acsami.8b04470.

[41] T. Wu, N. Kummer, K.J. De France, S. Campioni, Z. Zeng, G. Siqueira, J. Dong, G. Nyström, Nanocellulose-lysozyme colloidal gels via electrostatic complexation 251 (2021), https://doi.org/10.1016/j.carbpol.2020.117021 117021.

[42] N. Kummer, T. Wu, K.J. De France, F. Zuber, Q. Ren, P. Fischer, S. Campioni, G. Nyström, Self-Assembly Pathways and Antimicrobial Properties of Lysozyme in Different Aggregation States, Biomacromolecules. 22 (2021) 4327–4336, https://doi.org/10.1021/acs.biomac.1c00870.

[43] N.H.C.S. Silva, P. Garrido-Pascual, C. Moreirinha, A. Almeida, T. Palomares, A. Alonso-Varona, C. Vilela, C.S.R. Freire, Multifunctional nanofibrous patches composed of nanocellulose and lysozyme nanofibers for cutaneous wound healing, Int. J. Biol. Macromol. 165 (2020) 1198–1210, https://doi.org/10.1016/j.ijbiomac.2020.09.249.

[44] N.H.C.S. Silva, P. Figueira, E. Fabre, R.J.B. Pinto, M.E. Pereira, A.J.D. Silvestre, I.M. Marrucho, C. Vilela, C.S.R. Freire, Dual nanofibrillar-based bio-sorbent films composed of nanocellulose and lysozyme nanofibrils for mercury removal from spring waters, Carbohydr. Polym. 238 (2020), https://doi.org/10.1016/j.carbpol.2020.116210 116210.

[45] Y. Huang, P. Yang, F. Yang, C. Chang, Self-supported nanoporous lysozyme/nanocellulose membranes for multifunctional wastewater purification, J. Memb. Sci. 635 (2021), https://doi.org/10.1016/j.memsci.2021.119537 119537.

[46] J. Toro-Sierra, A. Tolkach, U. Kulozik, Fractionation of α-Lactalbumin and β-Lactoglobulin from Whey Protein Isolate Using Selective Thermal Aggregation, an Optimized Membrane Separation Procedure and Resolubilization Techniques at Pilot Plant Scale, Food Bioprocess Technol. 6 (2013) 1032–1043, https://doi.org/10.1007/s11947-011-0732-2.

[47] M. Usuelli, Y. Cao, M. Bagnani, S. Handschin, G. Nyström, R. Mezzenga, Probing the Structure of Filamentous Nonergodic Gels by Dynamic Light Scattering, Macromolecules. 53 (2020) 5950–5956, https://doi.org/10.1021/acs.macromol.0c00610.

[48] C.A. Schneider, W.S. Rasband, K.W. Eliceiri, NIH Image to ImageJ: 25 years of image analysis, Nat. Methods. 9 (2012) 671–675, https://doi.org/10.1038/nmeth.2089.
[49] Y. Cao, S. Bolisetty, J. Adamcik, R. Mezzenga, Elasticity in Physically Cross-Linked Amyloid Fibril Networks, Phys. Rev. Lett. 120 (2018), https://doi.org/10.1103/PhysRevLett.120.158103 158103.
[50] M.L. Gardel, J.H. Shin, F.C. MacKintosh, L. Mahadevan, P. Matsudaira, D.A. Weitz, Elastic behavior of cross-linked and bundled actin networks, Science. 304 (2004) 1301–1305, https://doi.org/10.1126/science.1095087.
[51] O. Lieleg, M.M.A.E. Claessens, C. Heussinger, E. Frey, A.R. Bausch, Mechanics of bundled semiflexible polymer networks, Phys. Rev. Lett. 99 (2007) 3–6, https://doi.org/10.1103/PhysRevLett.99.088102.
[52] Y.-C. Lin, N.Y. Yao, C.P. Broedersz, H. Herrmann, F.C. MacKintosh, D.A. Weitz, Origins of elasticity in intermediate filament networks, Phys. Rev. Lett. 104 (2010) 1–4, https://doi.org/10.1103/PhysRevLett.104.058101.
[53] F.C. Mackintosh, J. Kas, P.A. Janmey, Elasticity of Semi-flexible polymer networks, Phys. Rev. Lett. 75 (1995) 4425, https://doi.org/10.1103/PhysRevLett.75.4425.
[54] C.P. Broedersz, F.C. Mackintosh, Modeling semiflexible polymer networks, Rev. Mod. Phys. 86 (2014) 995–1036, https://doi.org/10.1103/RevModPhys.86.995.
[55] M.C.E. Van Dalen, J. Vaneyck, S.A. Semerdzhiev, M. Karperien, J.N. Post, M.M.A. E. Claessens, Protein Adsorption Enhances Energy Dissipation in Networks of Lysozyme Amyloid Fibrils, Langmuir. 37 (2021) 7349–7355, https://doi.org/10.1021/acs.langmuir.1c00657.
[56] L. Zhong, S. Fu, X. Peng, H. Zhan, R. Sun, Colloidal stability of negatively charged cellulose nanocrystalline in aqueous systems, Carbohydr. Polym. 90 (2012) 644–649, https://doi.org/10.1016/j.carbpol.2012.05.091.
[57] L. Geng, N. Mittal, C. Zhan, F. Ansari, P.R. Sharma, X. Peng, B.S. Hsiao, L.D. Söderberg, Understanding the Mechanistic Behavior of Highly Charged Cellulose Nanofibers in Aqueous Systems, Macromolecules. 51 (2018) 1498–1506, https://doi.org/10.1021/acs.macromol.7b02642.
[58] R.J. Hill, Elastic modulus of microfibrillar cellulose gels, Biomacromolecules. 9 (2008) 2963–2966, https://doi.org/10.1021/bm800490x.
[59] N. Quennouz, S.M. Hashmi, H.S. Choi, J.W. Kim, C.O. Osuji, Rheology of cellulose nanofibrils in the presence of surfactants, Soft Matter. 12 (2016) 157–164, https://doi.org/10.1039/c5sm01803j.
[60] L. Jowkarderis, T.G.M. Van De Ven, Rheology of semi-dilute suspensions of carboxylated cellulose nanofibrils, Carbohydr. Polym. 123 (2015) 416–423, https://doi.org/10.1016/j.carbpol.2015.01.067.